On the Impact of Local Feedbacks in the Central Pacific on the ENSO Cycle

GERRIT BURGERS AND GEERT JAN VAN OLDENBORGH

Royal Netherlands Meteorological Institute, De Bilt, Netherlands

(Manuscript received 18 April 2002, in final form 2 December 2002)

ABSTRACT

While sea surface temperature (SST) anomalies in the eastern equatorial Pacific are dominated by the thermocline feedback, in the central equatorial Pacific local wind effects, such as zonal advection, are important as well. El Niño–Southern Oscillation (ENSO) simulations with a linear model improve markedly if these effects are included as a local wind stress feedback on SST. An atmosphere model that reacts both to eastern and central Pacific SST anomalies is needed for producing a realistic ENSO cycle.

First, simulations are studied of a linear 1.5-layer reduced-gravity ocean model and a linear SST anomaly equation, forced by observed monthly wind stress. If only the thermocline feedback is present in the SST equation, SST can be simulated well in the eastern Pacific, but, contrary to observations, central Pacific SST is out of phase with the eastern Pacific. If a wind stress feedback is added in the SST equation, as a term proportional to the zonal wind stress, correlations between observed and simulated SST are above 0.8 in both the central and eastern Pacific, and the correlation between the Niño-3 (5°S–5°N, 90°–150°W) and Niño-4 (5°S–5°N, 150°W–160°E) indexes is close to the observed value of 0.75.

Next, a statistical atmosphere is added to the ocean module that is based on a regression of observed wind stress to the observed Niño-3 and Niño-4 indexes. The coupled system is driven by noise that is inferred from the residues of the fit and has a red component. The observed Niño-3–Niño-4 index correlation can be reproduced only with a wind stress feedback in the central Pacific. Also, the level of SST variability rises and the ENSO period increases to more realistic values.

The interplay between the local wind stress and the thermocline feedbacks, therefore, is an important factor in the structure of ENSO in the coupled linear model. In the eastern Pacific, the thermocline feedback dominates SST anomalies; in the central Pacific, the local wind stress feedback. Due to the local wind stress feedback, the ENSO wind stress response excites SST anomalies in the central Pacific, extending the ENSO SST anomaly pattern well into the central Pacific. In turn, these central Pacific SST anomalies give rise to wind stress anomalies that are situated more westward than the response to eastern Pacific SST anomalies. As a result, the ENSO amplitude is enhanced and the ENSO period increased. Also, central Pacific SST anomalies are not completely determined by eastern Pacific SST anomalies and they persist longer.

1. Introduction

Central to El Niño–Southern Oscillation (ENSO) are processes that control SST anomalies in the equatorial Pacific. Many authors have studied these processes and several mechanisms have been identified to be important: vertical advection by anomalous upwelling, vertical advection over an anomalous vertical temperature ingredient, and zonal advection of zonal temperature gradients. The subject of this paper is to investigate to what extent SST can be modeled by a linear SST equation, how the relative strengths of the processes vary with longitude, and how the characteristics of ENSO depend on the feedbacks in the central Pacific.

The thermocline feedback, that is, upwelling over an anomalous temperature gradient that accompanies a thermocline anomaly, is the most important feedback in the eastern Pacific, as has long been recognized (see, e.g., the study of Kleeman 1993). The relevance for ENSO of surface-layer feedbacks such as the zonal advection feedback was established in the study of Neelin (1991) of the slow SST mode. Seager (1989) pointed out that the feedbacks affect the central and eastern Pacific in a different way. Interest in the zonal advection feedback was renewed by Picaut et al. (1996, 1997) who stressed the importance of the zonal displacement of the Pacific warm pool for ENSO. Jin and An (1999) concluded that in a simple recharge oscillator model, the zonal advection feedback enhances the ENSO mode caused by the thermocline feedback. Simplified SST equations have been used in many studies of the mechanisms that play a role in El Niño; see for example, the review by Dijkstra and Burgers (2002). However, relatively few intermediate model studies make quantita-

Corresponding author address: Dr. Gerrit Burgers, Oceanographic Research, KNMI, P.O. Box 201, NL-3730 AE De Bilt, Netherlands. E-mail: burgers@knmi.nl

tive comparisons with observations, and most of those are restricted to comparisons with the Niño-3 index.[1] An exception is the study of Y.-Q. Chen et al. (1995). Also, there have been a number of papers that relate the effect of parameter variations in simple or intermediate models to observed changes in decadal ENSO behavior, such as the studies of Fedorov and Philander (2000, 2001) and An and Jin (2000).

In this paper, we study forced and coupled ENSO simulations of a linear anomaly model with simplified and linear SST physics. The thermocline feedback in the SST equation of the ocean model is incorporated as a linear feedback to thermocline depth anomaly, as in Kleeman (1993). We parameterize the zonal advection feedback by a method proposed by Latif (1987): through a term in the SST equation that is linear in the zonal wind stress anomaly. In the coupled runs, the atmosphere component consists of a statistical model that is driven by the Niño-3 and Niño-4 indices. The coupled model is driven by noise in the atmospheric component with properties estimated from observations. Seasonal cycle effects in the strength of the feedbacks and in the statistical atmosphere model are neglected in this study, in order to keep the analysis simple and the number of tunable parameters small. The ocean and the statistical atmosphere model, the wind stress forcing, and the SST data used for comparing model behavior to observed behavior are described in section 2. In section 3, forced ocean runs are discussed. SST in the central and eastern Pacific can be simulated quite well if both the thermocline and the local wind stress feedback are included in the SST equation. The coupled ocean–atmosphere runs presented in section 4 show much more realistic SST variability if both the thermocline and the wind stress feedbacks are included in the SST equation. The results and the implications for the role of the central Pacific in ENSO are discussed in section 5, followed by a conclusion.

2. Model, forcing, and data

The ocean component consists of a linear shallow-water model and a linear SST equation. The 1.5-layer shallow-water model of the upper Pacific Ocean gives the response of the thermocline depth to anomalies in the wind stress forcing. It has a limited domain with closed boundaries at 30°S and 30°N and realistic closed western and eastern boundaries. The shallow-water wave speed is 2.2 m s^{-1}. The model is described in more detail in Burgers et al. (2002).

The SST equation gives the response of SST to thermocline and wind stress anomalies. In the eastern Pacific, SST is closely related to the thermocline depth anomaly, because the latter is an indicator for the vertical transport of temperature anomalies by mean upwelling. This is modeled by a term linear in the thermocline anomaly, because in the Tropical Atmosphere Ocean/Triangle Trans-Ocean Buoy Network (TAO/TRITON) data (McPhaden et al. 1998) there is no indication of nonlinearities in scatterplots of thermocline depth versus SST anomalies. The coefficient of this term depends on longitude and is stronger in the eastern Pacific. The use of such an SST equation in a coupled model has been studied already by Kleeman (1993).

In the central Pacific, transport of the mean zonal temperature gradient by zonal velocity anomalies is more important. However, the representation of surface zonal velocity by a 1.5-layer shallow-water model is rather poor, even if an Ekman layer is added (Boulanger 2001). This can also be seen from monthly observations of wind and current of the TAO/TRITON array. West of 140°W, the correlation between observed zonal surface velocity and zonal wind is comparable or slightly better than the correlation between observed velocity and the velocity of the 1.5-layer linear model. For this reason, a term proportional to zonal wind stress is included in the SST equation, rather than a term proportional to model zonal velocity. An obvious disadvantage is that zonal velocity fluctuations that are not related to local zonal wind stress variations are not taken into account. An advantage is that anomalous upwelling and evaporation effects are included to some extent, as well as some of the negative radiation feedback from clouds discussed in Jin et al. (2001). A one-variable model with such a local wind stress feedback, representing the effects of locally forced vertical and zonal advection, was used in the study of Latif (1987) to model SST anomalies in the central Pacific. Here, we use a term in the SST equation with a coefficient that depends on longitude and reaches a maximum in the central Pacific, where the mean zonal temperature gradient is maximal.

The linear equation for SST anomalies, therefore, has the following generic form:

$$\frac{dT}{dt} = \alpha(x)h(x, y) + \beta(x)\tau^x(x, y) - \gamma(x)T(x, y) \quad (1)$$

with T the SST anomaly field, h the thermocline anomaly field, and τ^x the zonal wind stress forcing anomaly field; x denotes the zonal and y the meridional dependence. The factors α, β, and γ determine the strength of the feedbacks and the relaxation time, which vary considerably along the equator because of variations in the depth of the mean thermocline, mean upwelling, and mean zonal temperature gradient. Because we are mainly interested in the SST close to the equator, we have not attempted to make these factors dependent on latitude.

In order to avoid overtuning the factors $\alpha(x)$, $\beta(x)$, and $\gamma(x)$, we have restricted our search to functions that consist of two linear pieces or one quadratic piece. Tun-

[1] The Niño-3 index is the SST anomaly of the Niño-3 area 5°S–5°N, 150°–90°W; the Niño-3.4 index is the SST anomaly of the Niño-3.4 area, 5°S–5°N, 170°–120°W; and the Niño-4 index is the SST anomaly of the Niño-4 area 5°S–5°N, 160°E–150°W.

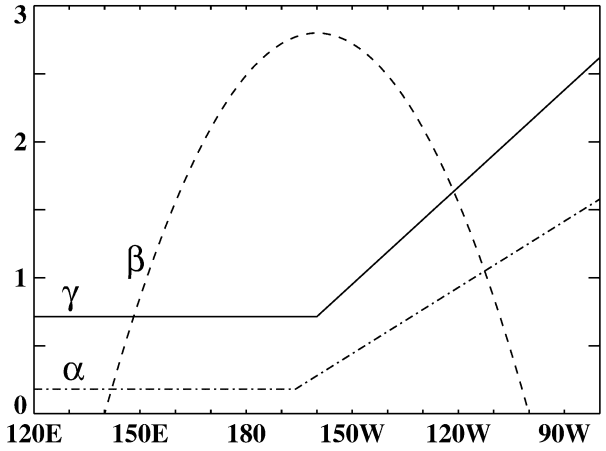

FIG. 1. Factors in the SST equation (1) as a function of longitude; here α is in units of K (10 m)$^{-1}$ month^{-1}, β in K (0.1 Pa)$^{-1}$ month^{-1}, and γ in month^{-1}.

ing is such that observed monthly SST along the equator over the period 1982–99 is reproduced best. The result is shown in Fig. 1. The gross features of the functional relationship of the factors are consistent with observational and model studies of the mechanisms that affect SST in the equatorial Pacific. Kang et al. (2001), in a budget study of the National Centers for Environmental Prediction–National Center for Atmospheric Research (NCEP–NCAR) reanalysis data, find that mean upwelling and zonal advection are the important terms and that meridional advection acts effectively as a damping term. Wang and McPhaden (2000, 2001) using TAO/TRITON data confirm the importance of zonal advection in the central Pacific and of vertical advection in the eastern Pacific. Vialard et al. (2001) reach similar conclusions from the analysis of an ocean general circulation model forced by TAO/TRITON data and *European Remote-Sensing Satellite-1/-2* (*ERS-1/-2*) wind stress fields. Although we expect β to be smaller in the eastern than in the central Pacific, probably this effect is exaggerated in our standard setting because we assumed a quadratic dependence for $\beta(x)$. Mean upwelling causes both α and γ to increase in the eastern Pacific. That α increases more rapidly than γ means that the equilibrium response of SST to a thermocline anomaly increases going eastward. The scale of the factors α, β, and γ is consistent with order-of-magnitude estimates that are obtained using the framework of the SST equation of Zebiak and Cane (1987) and are discussed below.

In the central Pacific, where the damping is mainly caused by anomalous surface fluxes, the magnitude of the relaxation factor γ is around (6 weeks)$^{-1}$. Assuming that temperature is well mixed to a depth H of approximately 50 m in this region, this value of γ is compatible with the estimates of Oberhuber (1988) for the relation between heat flux anomalies and SST anomalies of around 50 W m^{-2} K^{-1} in this region. An order of magnitude estimate for the factor β in this region is made by considering the idealized case of an Ekman layer of uniform depth, with linear damping, and forced by a constant zonal wind stress anomaly, as discussed, for example, in the textbook of Dijkstra (2000). Then, anomalous zonal advection of the mean zonal temperature gradient $u_E T_x$ gives $\beta \approx 17$ K Pa^{-1} month^{-1} for a mixed-layer depth $H_u = 20$ m for currents, an Ekman damping time $t_E = 1.5$ days, a zonal temperature gradient of $T_x = 1$ K (1000 km)$^{-1}$, and using that the zonal Ekman velocity is $u_E = t_E \tau^x / \rho H_u$ right at the equator (ρ is the density of seawater). Similarly, anomalous upwelling of the mean vertical temperature gradient $w_E T_z$ gives $\beta \approx 10$ K Pa^{-1} month^{-1} for an effective mean vertical temperature gradient of $\Delta T / H_u = 0.01$ K m^{-1}, and using that at the equator the Ekman upwelling velocity is given by $w_E = \beta_0 t_E^2 \tau^x / \rho$ (β_0 is the equatorial beta parameter). In the eastern Pacific, where thermocline anomalies are large, while wind stress anomalies are smaller than in the central Pacific, mean upwelling of anomalous temperature at the bottom of the mixed layer, $dT/dt = \overline{w} T'_Z$, dominates. Parameterizing $T'_z \sim (T'_s - T')/H$ with H the mixed-layer depth, $T'_s = ah'$, and a constant a, yields order of magnitude estimates for γ and α in this region. With $\overline{w} = 2$ m day^{-1}, $a = 0.05$ K m^{-1}, and $H = 30$ m in the eastern Pacific, one finds $\gamma = (15 \text{ days})^{-1}$ and $\alpha = 0.1$ K m^{-1} month^{-1}. Note that in this region, where the damping is mainly caused by upwelling, the relaxation time is much shorter than in the central Pacific.

In the forced runs in this paper, the model is forced with observed monthly wind stress anomalies from Florida State University (FSU; Stricherz et al. 1997). The results of SST simulations have been compared to observed data made available by NCEP: the observed monthly SST fields of Reynolds and Smith (1994) over the period 1982–99 and to observed Niño-3 and Niño-4 indexes (Reynolds and Smith 1994; Smith et al. 1996) over the period 1968–99.

The statistical atmosphere model is based on a linear regression from monthly observed FSU wind stress anomalies to the observed Niño-3 and Niño-4 indexes. The starting point are the regression patterns of the observed wind stress anomalies to the observed Niño indexes,

$$\mathbf{r}_3(x, y) = \overline{\boldsymbol{\tau}(x, y, t) N_3(t)} / \overline{N_3(t)^2} \tag{2}$$

$$\mathbf{r}_4(x, y) = \overline{\boldsymbol{\tau}(x, y, t) N_4(t)} / \overline{N_4(t)^2}, \tag{3}$$

where the overbars denote averages over time, $\boldsymbol{\tau}(x, y, t)$ is the wind stress vector field, and $N_3(t)$ and $N_4(t)$ stand for the Niño-3 and the Niño-4 indexes, respectively. Since $\boldsymbol{\tau}$ is a vector field, $\mathbf{r}_3$ and $\mathbf{r}_4$ are vector fields as well. As in Kirtman (1997), the regression pattern $\mathbf{r}_3$ could be used to construct a one-parameter estimate atmosphere based on the Niño-3 index and the pattern $\mathbf{r}_4$ for an estimate based on the Niño-4 index. For our statistical atmosphere model, we use a two-parameter

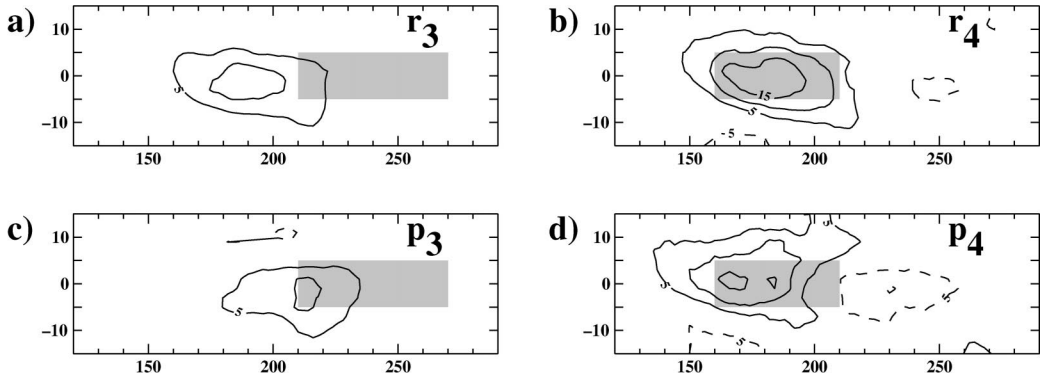

FIG. 2. FSU zonal wind stress regression patterns on (a) the Niño-3 index (r_3^x) and (b) the Niño-4 index (r_4^x), and statistical atmosphere patterns for (c) the Niño-3 (p_3^x) and (d) the Niño-4 indexes (p_4^x). Contour interval is 5 $m^2\ s^{-2}\ K^{-1}$.

estimate based on both the Niño-3 and the Niño-4 indexes:

$$\hat{\boldsymbol{\tau}}(x, y, t) = N_3(t)\mathbf{p}_3(x, y) + N_4(t)\mathbf{p}_4(x, y). \quad (4)$$

Here, the statistical atmosphere patterns $\mathbf{p}_3(x, y)$ and $\mathbf{p}_4(x, y)$ are such that the rms difference between $\hat{\boldsymbol{\tau}}(x, y, t)$ and $\boldsymbol{\tau}(x, y, t)$ is minimal. Because the Niño-3 and Niño-4 indexes are correlated, $\mathbf{p}_3$ and $\mathbf{p}_4$ are linear combinations of the regression patterns $\mathbf{r}_3$ and $\mathbf{r}_4$:

$$\begin{pmatrix}\mathbf{p}_3\\ \mathbf{p}_4\end{pmatrix} = \begin{pmatrix}\overline{N_3(t)^2} & \overline{N_3(t)N_4(t)}\\ \overline{N_3(t)N_4(t)} & \overline{N_4(t)^2}\end{pmatrix}^{-1}\begin{pmatrix}\overline{N_3(t)^2}\,\mathbf{r}_3\\ \overline{N_4(t)^2}\,\mathbf{r}_4\end{pmatrix}. \quad (5)$$

The regression and statistical atmosphere patterns for the zonal wind stress are shown in Fig. 2. The zonal component of the $\mathbf{p}_4$ pattern has a larger amplitude than that of $\mathbf{p}_3$, reflecting that SST anomalies of the warmer Niño-4 area have a stronger impact than anomalies of the same magnitude of the Niño-3 area. However, the impact of Niño-3 anomalies is roughly the same as that of Niño-4 anomalies, because Niño-3 variability is larger than Niño-4 variability.

Given the Niño-3 and Niño-4 indexes, the statistical atmosphere returns a wind stress anomaly as follows:

$$\boldsymbol{\tau}^{\text{stat}}(x, y, t) = [N_3(t) + \epsilon_3(t)]\mathbf{p}_3(x, y) + [N_4(t) + \epsilon_4(t)]\mathbf{p}_4(x, y), \quad (6)$$

where ϵ_3 and ϵ_4 are noise terms. In the coupled runs, the statistical atmosphere fields are updated four times per month. The statistical properties of the noise terms are estimated from the residues between $\hat{\boldsymbol{\tau}}$ and the projection of the FSU wind stress on the two patterns $\mathbf{p}_3$ and $\mathbf{p}_4$. Writing this projection as

$$\boldsymbol{\tau}^{\text{proj}}(x, y, t) = c_3(t)\mathbf{p}_3(x, y) + c_4(t)\mathbf{p}_4(x, y), \quad (7)$$

this means that ϵ_3 and ϵ_4 should statistically as much as possible behave as the residues $e_3(t) = c_3(t) - N_3(t)$ and $e_4(t) = c_4(t) - N_4(t)$ in amplitude, autocorrelation, and cross correlation. The amplitudes of the monthly $e_3(t)$ and $e_4(t)$ over 1968–99 are 0.61 and 0.43 K, respectively, while the cross correlation is 0.18. One set of coupled runs discussed in section 4 is driven by white noise with the same amplitude and cross correlation as the residues. However, the residues are not white in time: at a lag of one month, the autocorrelations of e_3 and e_4 are 0.50 and 0.24, respectively, and at a lag of 4 months they are 0.17 and 0.13, respectively. This indicates that a substantial red component is present in the residues if they are calculated as outlined above. In a very similar set up, Roulston and Neelin (2000) attribute the red component to SST variability outside the equatorial strip. A red component will also arise because the strength of the relation between the Niño index and the wind stress varies with the season and is not linear. Note that these explanations are not necessarily at variance with each other. In another set of coupled runs discussed in section 4, the runs are driven by a combination of white and red noise with roughly the same overall characteristics as the observed residues.[2]

If the ocean module is forced by the projection of the FSU wind anomalies on the two statistical atmosphere patterns, the variance of the simulated indexes is more than 73% of the variance in the standard run, while the correlations with the observed indexes are even higher than in the standard run. In runs driven by the projection on a single pattern, $\mathbf{r}_3$ or $\mathbf{r}_4$, correlations are still high but lower than in the run driven by the projection on two patterns. Also, the $\mathbf{r}_3$ pattern run explains only 42% of the Niño-4 variance, and the $\mathbf{r}_4$ pattern run explains only 55% of the Niño-3 variance.

The wind stress patterns of the statistical atmosphere (see Figs. 2c,d) have the same relative position to the Niño-3 and Niño-4 areas. This is not the case for the

[2] The random variable ϵ_3 is formed from a white and a red part. For a time step of 0.25 months the red part explains 60% of the variance, and the decay timescale of the red part is 2.5 months. For ϵ_4, the basis is a random variable r that again consists of a white and a red part, which in this case explains 30% of the variance and has a decay timescale of 3.6 months. The basis is combined with a small admixture of ϵ_3 such that the cross correlation at zero lag equals 0.18.

TABLE 1. Correlations between observed and modeled Niño indexes over the period 1968–99, and amplitudes (K).

	h only		τ only		h and τ		Observed	
	r	σ	r	σ	r	σ	r	σ
Niño-3	0.83	1.02	0.21	0.29	0.83	1.02	1	1.02
Niño-3.4	0.77	0.80	0.68	0.47	0.87	0.95	1	0.96
Niño-4	−0.13	0.63	0.85	0.68	0.84	0.69	1	0.68

regression patterns of Figs. 2a,b. The Gill model–type response (see e.g., Dijkstra 2000) of the two-parameter atmosphere patterns, with a maximum west of the center of the SST index area, shows that the two-parameter statistical estimate captures the physical relationship between SST anomalies and wind stress response better than the one-parameter estimates.

3. Forced runs

The SST equation of the model incorporates two feedbacks: the thermocline feedback and the wind stress feedback. In this section, results of three forced runs over the period 1968–99 are described: one run with only the thermocline feedback, one run with only the wind stress feedback, and one run with both feedbacks included. For simplicity, in the runs with only one feedback, the parameters of the SST equation were taken independent of longitude. In all cases, the free parameters were tuned for optimal results.

In the first run, only the thermocline feedback is included, so $\beta = 0$. The SST relaxation time is taken independent of longitude: $\gamma^{-1} = 2$ weeks, a value typical of the eastern Pacific; see Fig. 1. Taking much longer relaxation times gives worse results for the Niño-3 index (not shown). The thermocline feedback term α in (1) is taken independent of longitude as well. Its value, $\alpha = 0.151$ K m^{-1} month^{-1}, has been tuned such that the modeled standard deviation of the Niño-3 index is equal to the observed one. For the Niño-3, Niño-3.4, and Niño-4 indexes, correlations between observed and modeled values and standard deviations are shown in Table 1. A map of the correlation between observed and modeled SST is shown in Fig. 3a. In Table 2, cross

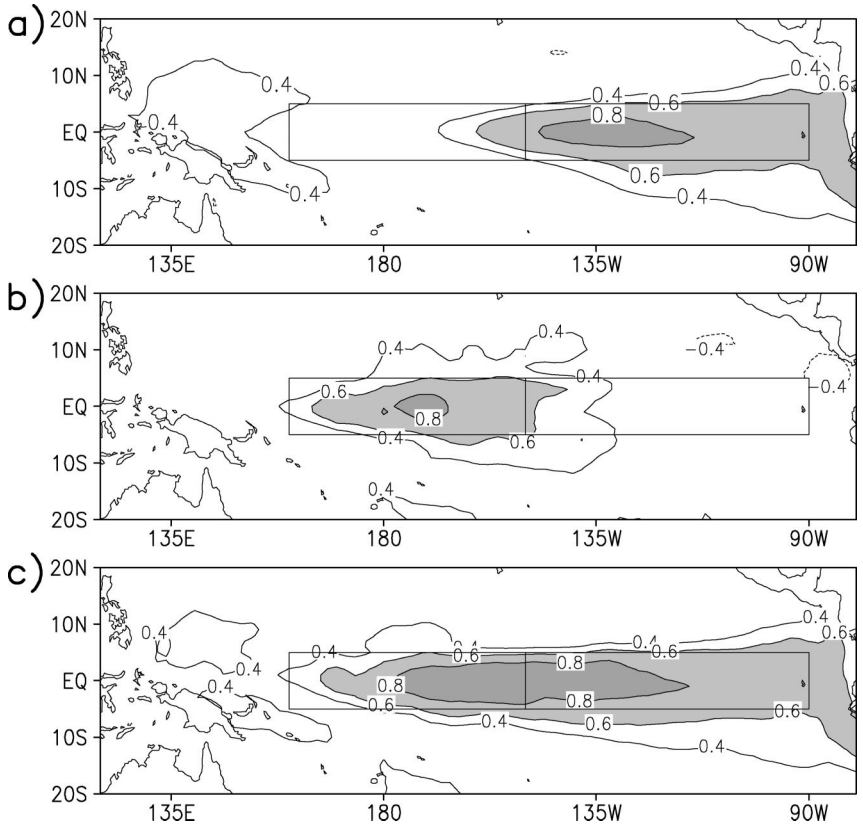

FIG. 3. Correlation between observed and modeled SST over the period 1982–99 for runs with (a) thermocline feedback only, (b) local wind stress feedback only, and (c) thermocline and local wind stress feedback. The boxes indicate the (left) Niño-4 and (right) Niño-3 areas.

TABLE 2. Cross-correlations of the modeled Niño indexes and of the observed Niño indexes over the period 1968–99.

	h only	τ only	h and τ	Observed
r (Niño-3, Niño-3.4)	0.85	0.66	0.95	0.95
r (Niño-3.4, Niño-4)	0.10	0.75	0.90	0.89
r (Niño-3, Niño-4)	−0.35	0.11	0.79	0.75

correlations of the modeled Niño indexes and of the observed Niño indexes are shown. Note that a longitude-dependent α gives the same correlation field. In the eastern Pacific, correlation between observed and modeled SST reaches values around 0.8, but in the central Pacific the agreement between observed and modeled SST is much lower. Another measure of the disagreement between model and data is that in the model the Niño-3 and Niño-4 indexes have a negative correlation of −0.35 while in the observations they have a positive correlation of 0.75 (see Table 2).

In the second run, only the wind stress feedback is included, so $\alpha = 0$. In this run the relaxation time γ^{-1} is 6 weeks, independently of longitude, a value appropriate for the central Pacific; see Fig. 1. The wind stress feedback term β in (1) is taken independent of longitude as well, with a $\beta = 34.2$ K Pa^{-1} month^{-1}, such that the modeled standard deviation of the Niño-4 index is equal to the observed one. In this case, in the central Pacific the agreement between observed and modeled SST is good, while in the eastern Pacific it is poor (see Table 1 and Fig. 3b). The correlation between the Niño-3 and Niño-4 indexes in this run is only 0.11. (see Table 2). Finally, the ratio of the amplitude of the Niño-3 index to that of the Niño-4 index is much smaller than observed, although with the constant value of β in this run, it is highly unlikely that the wind stress feedback is underestimated in the Niño-3 region compared to the Niño-4 region.

In the third run, the standard setting of Fig. 1 for the factors α, β, and γ has been used, which has been discussed in section 2. In this run, the agreement between observed and modeled SST is good both in the eastern Pacific and central Pacific and the amplitude of the Niño indexes is close to observed (see Table 1 and Fig. 3c), while the correlation between the Niño-3 and Niño-4 indexes in this run is also close to observed (see Table 2).

The autocorrelations of the time series of the Niño-3, the Niño-3.4, and the Niño-4 index for the three runs are shown together with the observed autocorrelation in Fig. 4. Only the run with both thermocline and wind stress feedback is reasonably close to the observations for all three indexes. Note that the sampling uncertainty in establishing the autocorrelation from a limited stretch of data varies considerably with the lag. For example, at short lags, where the autocorrelation is of the order of 0.9, the 95% confidence limits are of the order of ±0.02, while for large lags, where the autocorrelation is not much different from zero and the effective number

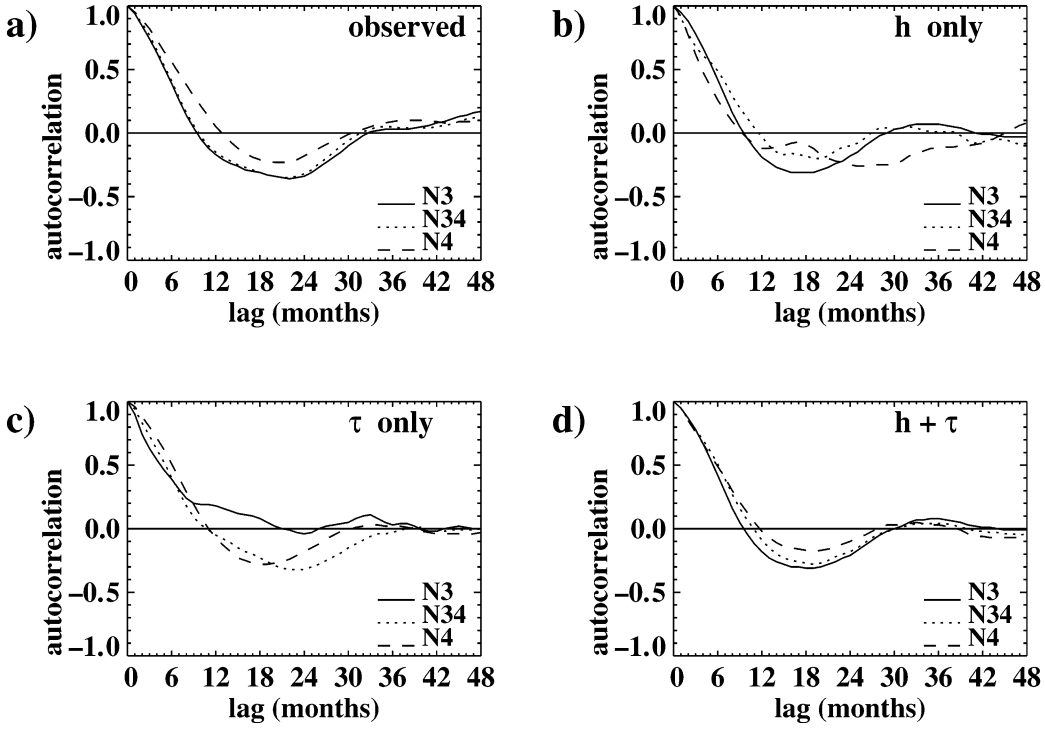

FIG. 4. Autocorrelation functions of the Niño-3, Niño-3.4, and Niño-4 indexes in forced runs over the period 1968–99 for (a) the observations, (b) a run with thermocline feedback only, (c) a run with wind stress feedback only, and (d) a run with both thermocline and wind stress feedback.

TABLE 3. Cross correlations and amplitudes (K) of the Niño indexes in coupled runs and observations.

	h only white	τ only white	h and τ white	h only white + red	τ only white + red	h and τ white + red	Observed
r (Niño-3, Niño-3.4)	0.66	0.76	0.96	0.62	0.72	0.96	0.95
r (Niño-3.4, Niño-4)	0.53	0.50	0.90	0.49	0.47	0.91	0.89
r (Niño-3, Niño-4)	−0.18	−0.19	0.78	−0.29	−0.28	0.79	0.75
σ (Niño-3)	0.28	0.10	0.64	0.42	0.13	1.03	1.02
σ (Niño-3.4)	0.22	0.16	0.63	0.28	0.22	1.00	0.96
σ (Niño-4)	0.14	0.26	0.48	0.23	0.37	0.76	0.68

of degrees of freedom is smaller, the 95% confidence limits are of the order of ± 0.25. So especially statistically significant are the underestimates at short lags of the Niño-4 autocorrelation in the thermocline-only run, and of the Niño-3 autocorrelation in the wind stress–only run.

In a related paper (Zelle et al. 2002, manuscript submitted to *J. Phys. Oceanogr.*, hereafter Z02), the time lag between equatorial thermocline depth and SST anomalies has been studied in observations, in a GCM simulation, and in the same intermediate model. The characteristic structure of the time lag, which is a function of longitude, is reproduced in the intermediate model only if the local wind stress feedback is added.

4. Coupled runs

In the coupled runs, the ocean model is coupled to the statistical atmosphere described in section 2. This statistical atmosphere is based on two wind stress patterns and is driven by the Niño-3 and Niño-4 indexes plus noise terms that have the same amplitude as the residues of the projection of the observed wind stress on the statistical atmosphere patterns. In the first set of runs discussed here, the noise terms are white in time, which is not quite true for the observed residues. As in the previous section, three runs are compared. In the first run, only the thermocline feedback is included: $\alpha = \alpha(x)$, $\gamma = \gamma(x)$ as in Fig. 1, and $\beta = 0$. In a forced run, this choice gives a good simulation of the Niño-3 index ($\sigma = 0.94$, $r = 0.83$) and suppresses the Niño-4 index that is simulated badly ($\sigma = 0.28$, $r = 0.10$). In the second run, only the wind stress feedback is included with a constant relaxation factor: $\alpha = 0$, $\beta = \beta(x)$ as in Fig. 1, and $\gamma^{-1} = 6$ weeks. In a forced run, this choice gives a good simulation of the Niño-4 index ($\sigma = 0.67$, $r = 0.84$) and suppresses the Niño-3 index that is simulated less well ($\sigma = 0.21$, $r = 0.44$). In the third run, both feedbacks are included with the standard setting for $\alpha(x)$, $\beta(x)$, and $\gamma(x)$ of Fig. 1. The duration of the runs was 250 years.

The cross correlations of the Niño indices are are shown in in Table 3, as well as the amplitudes of the Niño indices. The observed positive correlation between the Niño-3 and Niño-4 indexes is reproduced only in the run with both the thermocline and wind stress feedback. The autocorrelation functions of the Niño indexes in the coupled runs are shown in Fig. 5. For the run with both feedbacks, the autocorrelation functions shown in Fig. 5a are similar to the observed autocorrelations shown in Fig. 4a. For the run with only the thermocline feedback (see Fig. 5b) the broad features of the Niño-3 autocorrelation are similar, although the dominating timescale is shorter, while the Niño-4 autocorrelation function is quite different from observed. The autocorrelation functions in the run with only wind stress feedback are quite different from observed; see Fig. 5c. While in all runs the amplitudes are much smaller than observed, the underestimation is most severe in the runs with only one of the feedbacks included.

The amplitude is partly underestimated because the approximation that the driving noise is white in time is not very good. We have made a second set of runs where the driving noise consists of a combination of a white and red component, which better approximates the autocorrelation of the observed residues (see section 2). In this set of runs, the Niño-3–Niño-4 correlation is close (0.79) to the observed correlation (0.75) if both feedbacks are included, but very different (<0) if only one feedback is included. The amplitudes of the Niño-3, Niño-3.4, and Niño-4 indexes are close to the observed values in the run with both feedbacks included, but much smaller in the runs with only one feedback included (see Table 3). The autocorrelations of the run with both feedbacks are shown in Fig. 5d. The general features are similar as in the white-noise-driven run; at short lags the correlations are higher and closer to the observed values. The minimum of autocorrelation function is lower than observed, corresponding to a spectrum that is more peaked. The dominating timescale, estimated from the position of the zeroes of the autocorrelation function, is around 3 yr, which is close to the timescale of the forced run and slightly shorter than observed (see Figs. 4a,d).

Time–longitude diagrams for equatorial SST in the runs forced by the combination of white and red noise are shown in Fig. 6. For comparison, a time–longitude diagram of observed equatorial SST anomalies over a period of the same length is shown as well. SST anomalies propagate eastward in the thermocline feedback run, and westward in the wind stress feedback run. Westward propagation in the latter is possible because the statistical atmosphere is based on two patterns rather than one. The spatial and temporal structure of the run

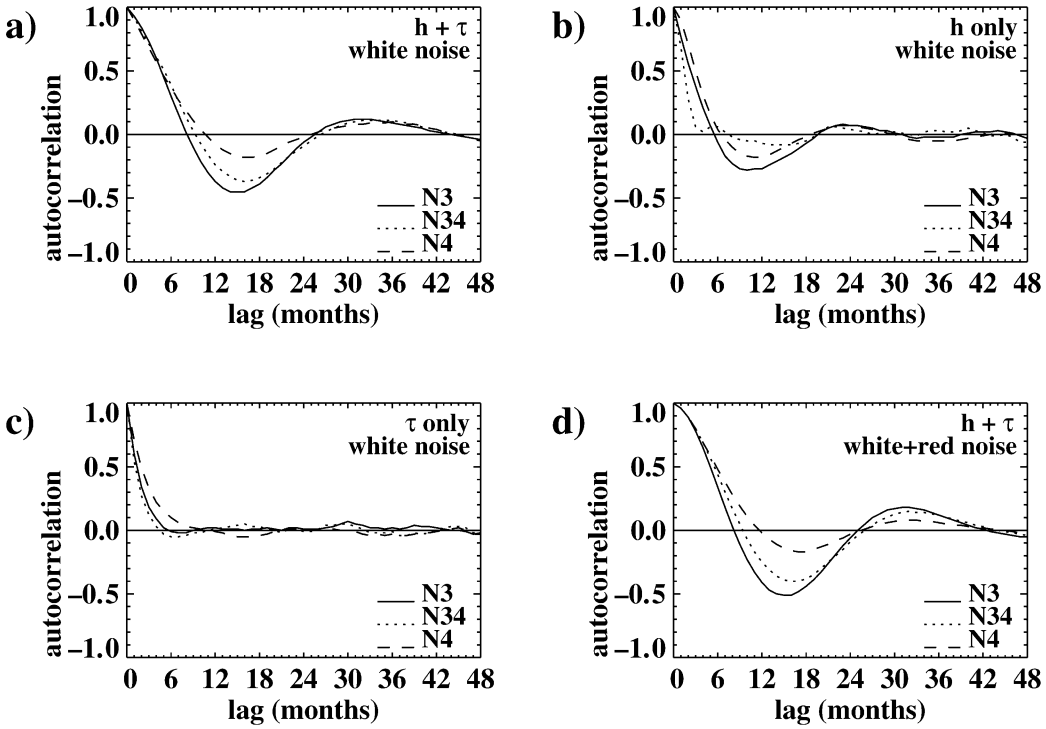

FIG. 5. Autocorrelation functions for the Niño-3, Niño-3.4, and Niño-4 indexes in 250-yr coupled runs for (a) a run with both thermocline and wind stress feedback, (b) a run with only thermocline feedback, (c) a run with only wind stress feedback, and (d) a run with both thermocline and wind stress feedbacks and driven by a combination of white and red noise. The autocorrelation functions of the observed Niño indices are shown in Fig. 4a.

with both feedbacks is rather similar to the pattern of the observations, although the observations contain, of course, more variability at small spatial scales.

A simple way to increase the amplitude and period of white-noise-driven runs is to make the ocean–atmosphere coupling stronger. However, this deteriorates many other aspects of the simulation. Increasing the wind stress response to SST by 15% gives a Niño-3 amplitude close to observed (1.06) in the coupled model with both feedbacks, but the resulting correlation and autocorrelations are rather different from observed: a Niño-3–Niño-4 correlation of 0.87, and a Niño-3 autocorrelation that has a minimum of -0.59. The dominating period is 45 months, longer than in the case of the red-plus white-noise-driven run. The period is much shorter if only one of the feedbacks is included and the coupling increased: 21 months for the thermocline feedback-only case and 22 months for the wind stress feedback–only case.

To assess the importance of the two-parameter atmosphere, we also made runs driven by a one-parameter atmosphere based on the Niño-3 regression pattern $\mathbf{r}_3$. In the first of these runs, both feedbacks were included in the SST equation. The autocorrelation function of the Niño-3 index in this coupled run is of comparable quality as when the two-parameter atmosphere is used. However, the connection between the Niño-3 and Niño-4 indexes is too strong, with a correlation of around 0.95, if driven by red plus white noise, and the difference between the persistence of the Niño-3 and the Niño-4 indexes is too small. In the second of these runs, only the thermocline feedback was included in the SST equation. Niño-4 is anticorrelated with Niño-3 in this run and not simulated well, but the Niño-3 period is actually better than if the two-parameter atmosphere is used. Probably, this is because the pattern $\mathbf{r}_3$ captures some of the physical Niño-4 response through the statistical connection between Niño-3 and Niño-4, while the two-parameter atmosphere calculates the Niño-4 response to a poorly simulated Niño-4 index.

A sensitivity study was done that follows the study of An and Jin (2000) of decadal changes with a two-strip ENSO model. In model run I (II), the thermocline feedback is decreased (increased) with 12.5% and the wind stress feedback increased (decreased) with 5% with respect to the standard run. These changes reflect to some extent the difference of the mean state of the decade 1981–91 (1965–75) with respect to the long-term mean; see An and Jin (2000). Both runs are driven by the same realization of red plus white noise as the standard run. In model run I, with decreased thermocline feedback, Niño-3 amplitudes are smaller (76%), the ratio of the Niño-4 amplitude to the Niño-3 amplitude is larger, and the correlation between Niño-3 and Niño-4 indexes is higher (0.81) than in the standard run. The wind stress response pattern to the Niño-3 index is shift-

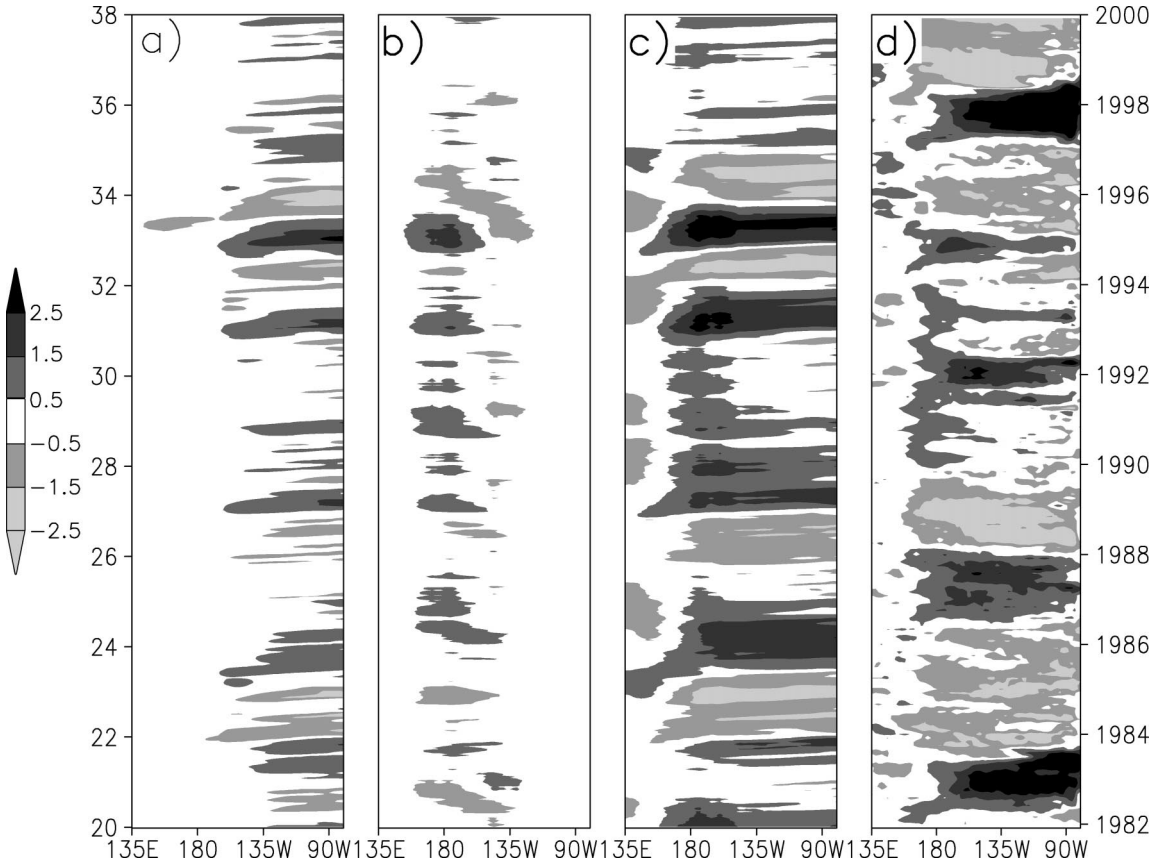

FIG. 6. Representative time–longitude diagrams of equatorial SST anomalies (K) in three coupled runs. Shown are 18-yr periods of coupled models driven by a combination of white and red noise, that have an ocean component with (a) only thermocline feedback, (b) only wind stress feedback, and (c) both thermocline and wind stress feedbacks. The atmospheric component is driven by the same noise realization in all three cases. (d) For comparison, the observations for the 18-yr period 1982–99 are shown.

ed to the west with respect to the standard run, and there is a larger tendency for westward propagation of SST anomalies. In model run II, with increased thermocline feedback, the reverse effects are observed: increased Niño-3 variability (137%), smaller Niño-4 to Niño-3 amplitude ratio, smaller (0.75) correlation between Niño-3 and Niño-4 indexes, eastward-shifted wind-response pattern, and more eastward propagation of SST anomalies. This is consistent with the results of Wang and An (2001, 2002), who study the effect in the Cane–Zebiak model (Zebiak and Cane 1987) of background changes induced by changes in the background wind stress. The effect on the period was relatively small; the period in run I is a few months larger than in run II.

5. Discussion

In the previous sections, it has been addressed how well SST variability in the central and eastern Pacific can be simulated by a linear thermocline depth model, a linear SST equation, and a noise-driven statistical atmosphere. The statistical atmosphere is based on two wind stress patterns that give the response to Niño-3 and Niño-4 index anomalies. Influences on SST are described by two ''shortcuts'' in the SST equation: direct, linear connections to thermocline depth and local zonal wind stress. The former is more important in the eastern Pacific, the latter in the central Pacific. That these feedbacks dominate so much and that they impact geographically separate regions are new aspects of the present study. Note that the distinction between local wind stress and thermocline feedback does not coincide with the distinction between zonal and vertical advection contributions in budget studies. For instance, in the eastern Pacific, transient zonal advection is correlated with thermocline variations (Jin and An 1999), while zonal wind stress anomalies in the central Pacific not only cause anomalous zonal advection but anomalous upwelling as well.

The factors in the SST equations were tuned to reproduce observations best in forced runs. Such a procedure can lead to overtuning, that is, an incorrect setting of parameters because of incomplete inclusion of physics, drawing inferences from too little data, or confusing cause and effect relationships. In particular, this is the case for the wind stress feedback in the central

Pacific, because central Pacific SST is correlated with eastern Pacific SST, which influences central Pacific wind stress. However, the correlations to the eastern Pacific are too low to explain the high correlation between simulated and observed SST in the central Pacific. Also, the nature of the physical relationships that have been discussed in section 2 makes it plausible that there is a wind stress feedback in the central Pacific. The risk of a circular argument becomes even more acute in the coupled system, as regression of observed zonal wind stress to the Niño-4 index leads to a pattern that almost coincides with the Niño-4 area; see Fig. 2b. It would therefore not be appropriate to use a statistical atmosphere based on the Niño-4 index only. However, the wind stress patterns of the statistical atmosphere (see Figs. 2c,d) seem to represent the physical effect of SST on wind stress, because they have the same relative position to the Niño-3 and Niño-4 areas, and resemble the physical pattern of a Gill model type of response with a maximum west of the center of the SST index area, as shown, for example, in the textbook of Dijkstra (2000).

Our forced runs show that the local wind stress feedback in the central Pacific is the key to a good simulation of the Niño-4 index, and that if both feedbacks are included, SST in the central and eastern Pacific can be simulated well. The correlation of 0.87 between the observed and simulated Niño-3.4 index is among the highest reported in the literature for simulations that do not use observed SST or thermocline data (see e.g., Y.-Q. Chen et al. 1995; D. Chen et al. 1995; Kirtman and Schneider 1996; Kang and Kug 2000), although the linear model does not include important effects such as seasonality and nonlinearities. The wind stress feedback makes the Niño-4 index more persistent and less oscillatory than the Niño-3 index. The interplay between local wind stress feedback and thermocline feedback results in a correlation between Niño-3 and Niño-4 indexes close to the observed value of around 0.75. As shown by Z02, the simulation of the lag relationship between local thermocline and SST anomalies improves as well if the local wind stress feedback is included.

In coupled runs driven by white noise, the amplitude is underestimated severely. This could be due to several reasons. The coupling could be underestimated in the construction of the linear statistical atmosphere, or the real ENSO system might less stable with respect to small perturbations than with respect to large ones. Another reason is that the probability density function of the residues of the statistical atmosphere is not white in time, but has a red component, as noted by Roulston and Neelin (2000). As explained in section 2, such a red component in the residues could be to some extent an artifact, because we use a statistical atmosphere without an annual cycle. The effect of adding a red component to the noise differs from that of increasing the coupling strength in a system driven by white noise. In the latter case, increasing the coupling until amplitudes reach observed values results in oscillations that are much more regular than in the case with red noise added.

In limiting cases, the coupled system shows the two types of modes that play an important role in ENSO and are, for example, discussed in the review of Neelin et al. (1998): delayed oscillator modes if only the thermocline feedback is included, and SST modes if only the local wind stress feedback is included. The two statistical atmosphere patterns make a westward-propagating SST mode possible, as shown in Fig. 6b, with positive Niño-3 anomalies causing a positive Niño-4 tendency, and positive Niño-4 anomalies a negative Niño-3 tendency. The period of both the delayed-oscillator mode and of the SST mode is around 2 yr, and the SST variability of the SST mode is concentrated much more westward than that of the delayed-oscillator mode, as in the study of Fedorov and Philander (2001).

If both feedbacks are included, a mixed mode is the result. Note that while we stress the importance of the local wind stress feedback, in our model the thermocline feedback is essential for the ENSO cycle, while in Picaut et al. (1997) it is the part of the zonal wind stress out of phase with the local wind stress. In contrast to the system of Fedorov and Philander (2001), in our system the parameterization of the feedbacks is such that the period is longer if both feedbacks are included than if only one feedback is included. The correlation between the Niño-3 and Niño-4 indexes in the simulation is close to observed. Driving the system by a combination of white and red noise with similar properties as observed residues gives Niño index amplitudes close to observed. The time–longitude diagram of equatorial SST of this coupled run shares many characteristics with a time–longitude diagram of observed SST, although the dominating period is shorter than observed and the cycles are still too regular. Episodes vary in strength and duration, and prolonged periods with persistent SST anomalies in the central Pacific occur. Altogether, the linear system seems able to simulate ENSO SST anomalies reasonably well, provided that both feedbacks are included and the system is driven by noise with the same characteristics as observed. Sensitivity experiments show that relatively small changes in the feedbacks (of the order of 10%) can lead to much larger changes in the amplitude (of the order of 30%), although the period is hardly affected. Experiments with different statistical atmospheres of the thermocline feedback model indicate that the atmospheric response has a large effect on the period.

The following picture emerges from the coupled runs. Wind stress anomalies excited by eastern Pacific SST or noise give rise to SST anomalies in the central Pacific because of the local wind stress feedback. Compared to the case with no local wind stress feedback in the central Pacific, this extends the spatial pattern of ENSO SST anomalies from the eastern Pacific well into the central Pacific and makes the system less stable. In turn, the ENSO wind stress pattern also extends more to the west,

and the period becomes longer. Niño-4 SST anomalies are not coupled completely to Niño-3 anomalies and persist longer, because different mechanisms influence SST in the Niño-3 and Niño-4 regions, and because wind stress in the Niño-4 region is not completely determined by Niño-3 anomalies.

6. Conclusions

Simulations of ENSO-related SST anomalies with a linear model improve markedly if a local wind stress feedback is added to the thermocline feedback in the SST equation, both in forced and coupled runs. The coupled system consists of a linear 1.5-layer shallow-water model, a linear SST equation, and a statistical atmosphere and is driven by noise added to the statistical atmosphere. The local wind stress feedback, which represents anomalous zonal advection and other local effects, is important in the central Pacific. The thermocline feedback dominates in the eastern Pacific.

In runs forced by observed wind stress anomalies, the ocean model simulates equatorial SST anomalies in the central and eastern Pacific quite well, with correlations well above 0.8 over the period 1968–99. The observed correlation between the Niño-3 and the Niño-4 indexes, which is of the order of 0.75, can only be properly simulated if the wind stress feedback is included.

Also, in noise-driven coupled runs, the observed Niño-3–Niño-4 correlation is reproduced only if both feedbacks are included. Amplitudes attain realistic values only if both feedbacks are included and if a red component, estimated from observations, is included in the noise that drives the system. Due to the local wind stress feedback in the central Pacific, the spatial pattern of ENSO is not confined to the eastern Pacific but extends into the central Pacific. In turn, compared to the situation with only thermocline feedback, the wind stress pattern of ENSO extends more to the west as well. The model period is longer, and the system is less stable. As observed, modeled SST anomalies are more persistent in the central than in the eastern Pacific.

Acknowledgments. Many discussions with Henk Dijkstra are gratefully acknowledged. Jorg Eij has assisted in testing early versions of the stochastically driven coupled model.

REFERENCES

An, S.-I., and F.-F. Jin, 2000: An eigen analysis of the interdecadal changes in the structure and frequency of ENSO mode. *Geophys. Res. Lett.,* **27,** 2573–2576.

Boulanger, J.-P., 2001: The Trident Pacific Model. Part I: Simulating surface ocean currents with a linear model during the 1993–1998 TOPEX/Poseidon period. *Climate Dyn.,* **17,** 159–173.

Burgers, G., M. A. Balmaseda, F. C. Vossepoel, G. J. van Oldenborgh, and P. J. van Leeuwen, 2002: Balanced ocean-data assimilation near the equator. *J. Phys. Oceanogr.,* **32,** 2509–2519.

Chen, D., S. Zebiak, A. Busalacchi, and M. Cane, 1995: An improved procedure for El Niño forecasting: Implications for predictability. *Science,* **269,** 1699–1702.

Chen, Y.-Q., D. S. Battisti, and E. S. Sarachik, 1995: A new ocean model for studying the tropical oceanic aspects of ENSO. *J. Phys. Oceanogr.,* **25,** 2065–2089.

Dijkstra, H. A., 2000: *Nonlinear Physical Oceanography.* Kluwer, xii and 456 pp.

——, and G. Burgers, 2002: Fluid dynamics of El Niño variability. *Annu. Rev. Fluid Mech.,* **34,** 531–558.

Fedorov, A. V., and S. G. H. Philander, 2000: Is El Niño changing? *Science,* **288,** 1997–2002.

——, and ——, 2001: A stability analysis of tropical ocean–atmosphere interactions: Bridging measurements and theory for El Niño. *J. Climate,* **14,** 3086–3101.

Jin, F.-F., and S.-I. An, 1999: Thermocline and zonal advective feedbacks within the equatorial ocean recharge oscillator model for ENSO. *Geophys. Res. Lett.,* **26,** 2989–2992.

——, Z.-Z. Hu, M. Latif, L. Bengtsson, and E. Roecker, 2001: Dynamical and cloud-radiation feedbacks in El Niño and greenhouse warming. *Geophys. Res. Lett.,* **28,** 1539–1542.

Kang, I.-S., and J.-S. Kug, 2000: An El-Niño prediction system using an intermediate ocean and a statistical atmosphere. *Geophys. Res. Lett.,* **27,** 1167–1170.

——, S.-I. An, and F.-F. Jin, 2001: A systematic approximation of the SST anomaly equation for ENSO. *J. Meteor. Soc. Japan,* **79,** 1–10.

Kirtman, B. P., 1997: Oceanic Rossby wave dynamics and the ENSO period in a coupled model. *J. Climate,* **10,** 1690–1704.

——, and E. Schneider, 1996: Model-based estimates of equatorial Pacific wind stress. *J. Climate,* **9,** 1077–1091.

Kleeman, R., 1993: On the dependence of the hindcast skill on ocean thermodynamics in a coupled ocean–atmosphere model. *J. Climate,* **6,** 2012–2033.

Latif, M., 1987: Tropical ocean circulation experiments. *J. Phys. Oceanogr.,* **17,** 246–263.

McPhaden, M. J., and Coauthors, 1998: The Tropical Ocean-Global Atmosphere observing system: A decade of progress. *J. Geophys. Res.,* **103,** 14 169–14 240.

Neelin, J. D., 1991: The slow sea surface temperature mode and the fast-wave limit: Analytic theory for tropical interannual oscillations and experiments in a hybrid coupled model. *J. Atmos. Sci.,* **48,** 584–606.

——, D. S. Battisti, A. C. Hirst, F.-F. Jin, Y. Wakata, T. Yamagata, and S. E. Zebiak, 1998: ENSO theory. *J. Geophys. Res.,* **103,** 14 261–14 290.

Oberhuber, J., 1988: An atlas based on the 'COADS' dataset: The budgets of heat, buoyancy and turbulent kinetic energy at the surface of the global ocean. MPI Rep. 15, Max Planck Institute of Meteorology, Hamburg, Germany, 202 pp.

Picaut, J., M. Ioualalen, C. Menkes, T. Delcroix, and M. J. McPhaden, 1996: Mechanism of the zonal displacements of the Pacific Warm Pool: Implications for ENSO. *Science,* **274,** 1486–1489.

——, I. Masia, and Y. du Penhoat, 1997: An advective-reflective conceptual model for the oscillatory nature of ENSO. *Science,* **277,** 663–666.

Reynolds, R. W., and T. M. Smith, 1994: Improved global sea surface temperature analyses using optimum interpolation. *J. Climate,* **7,** 929–948.

Roulston, M. S., and J. D. Neelin, 2000: The response of an ENSO model to climate noise, weather noise and intraseasonal forcing. *Geophys. Res. Lett.,* **27,** 3723–3726.

Seager, R., 1989: Modeling tropical Pacific sea surface temperature: 1970–87. *J. Phys. Oceanogr.,* **19,** 419–434.

Smith, T. M., R. W. Reynolds, R. E. Livezey, and D. C. Stokes, 1996: Reconstruction of historical sea surface temperatures using empirical orthogonal functions. *J. Climate,* **9,** 1403–1420.

Stricherz, J. N., D. M. Legler, and J. J. O'Brien, 1997: *Pacific Ocean.*

Vol. 2. TOGA Pseudo-Stress Atlas 1985–1994. Florida State University, 158 pp.

Vialard, J., C. Menkes, J.-P. Boulanger, P. Delecluse, E. Guilyardi, M. J. McPhaden, and G. Madec, 2001: A model study of oceanic mechanisms affecting equatorial Pacific sea surface temperature during the 1997–98 El Niño. *J. Phys. Oceanogr.*, **31,** 1649–1675.

Wang, B., and S. I. An, 2001: Why the properties of El Niño changed during the late 1970s. *Geophys. Res. Lett.,* **28,** 3709–3712.

——, and ——, 2002: A mechanism for decadal changes of ENSO behavior: Roles of background wind changes. *Climate Dyn.,* **18,** 475–586.

Wang, W., and M. McPhaden, 2000: The surface-layer heat balance in the equatorial Pacific Ocean. Part II: Interannual variability. *J. Phys. Oceanogr.,* **30,** 2989–3008.

——, and ——, 2001: Surface-layer temperature balance in the equatorial Pacific during the 1997–98 El Niño and the 1998–99 La Niña. *J. Climate,* **14,** 3393–3407.

Zebiak, S. E., and M. A. Cane, 1987: A model of El Niño–Southern Oscillation. *Mon. Wea. Rev.,* **115,** 2262–2278.